

# Oxygen-dosage effect on the structure and composition of ultrathin NiO layers reactively grown on Ag(001)

C. Giovanardi,<sup>1,\*</sup> A. di Bona,<sup>1</sup> and S. Valeri<sup>1,2</sup><sup>1</sup>*INFN, National Research Center on nanoStructures and bioSystems at Surfaces (S3), UdR di Modena, Via Campi 213/a, 41100-Modena, Italy*<sup>2</sup>*Dipartimento di Fisica, Università di Modena e Reggio Emilia, Via Campi 213/a, 41100-Modena, Italy*

(Received 19 March 2003; published 27 February 2004)

NiO ultrathin films have been prepared under UHV conditions on Ag(001) substrate by metal deposition in O<sub>2</sub> atmosphere. The films were prepared by deposition of the amount of metal correspondent to 1 ML (monolayer) of NiO in the presence of different oxygen-to-metal flux ratios, to investigate the oxygen dosage effect on the structure and composition of the growing layer and on the stoichiometry of Ni oxide. Thicker films (up to 20 ML) were also prepared. The structure has been monitored both in reciprocal and direct space by low-energy electron diffraction and primary-beam diffraction-modulated electron emission. Core-level x-ray photoemission spectroscopy has been used to study film chemistry and composition. At low coverage (below 2 ML) a dramatic dependence of structure and composition on the oxygen-to-nickel flux ratio has been observed. Low oxygen dosage induces a (2×1) reconstruction in the 1-ML films that evolves to a (1×1) phase as the dosage and/or the film thickness increases. In the layers prepared at low oxygen dosage a large fraction of metallic Ni coexists with the Ni oxide, but the oxidized fraction largely prevails for high oxygen dosage. The oxygen dosage during the growth also affects thicker films. The mosaic formation, which has been ascribed to misfit strain relaxation, is related to a low oxygen-to-nickel flux ratio.

DOI: 10.1103/PhysRevB.69.075418

PACS number(s): 68.35.-p, 61.14.-x, 68.55.-a, 82.80.Pv

## INTRODUCTION

Epitaxial growth of NiO films provides the opportunity to prepare materials specifically oriented to a large number of applications both in catalysis<sup>1,2</sup> and in magnetic nanodevices technology.<sup>3</sup> NiO is also a very appealing material for fundamental studies of electron correlation in solids.<sup>4,5</sup> In particular, in the monolayer thickness limit, the reduced Madelung potential and asymmetric environment could yield new electronic and magnetic properties of interest both theoretically and technologically.<sup>6</sup> Well-ordered and smooth NiO films are obtained by evaporating Ni in an oxygen atmosphere on substrates whose lattice parameter is close to that of NiO. In particular, the (100) surface of Ag was found to be an ideal substrate for the NiO epitaxy, because of the low reaction kinetic of oxygen on Ag and of the low mismatch (2%) between the fcc metal and rocksalt oxide. The structure and morphology of NiO films on the Ag(001) substrate have already been investigated by low-energy electron diffraction (LEED) and Auger and photoelectron electron diffraction,<sup>7-9</sup> scanning tunneling microscopy (STM),<sup>10,11</sup> spot profile analysis (SPA) LEED,<sup>12</sup> primary-beam diffraction-modulated electron emission (PDME),<sup>13</sup> and specular x-ray reflectivity.<sup>14</sup> For thin films, NiO were reported to grow layer by layer, in an initially pseudomorphic, tetragonally distorted rocksalt phase with the NiO(001)//Ag(001) and NiO[100]//Ag[100] epitaxial relationships with the Ag substrate. As the thickness of the oxide increases, the formation of mosaics on the film surface has been observed and ascribed to the process of relaxation of the misfit strain. A significant substrate disruption was observed by STM.

STM studies of submonolayer deposits show that a 2×1 structure (in two orthogonal domains) is formed after the

deposition of Ni at room temperature (RT) in an oxygen atmosphere.<sup>10,11</sup> This structure evolves in two-layer-thick NiO islands upon annealing. A 2×1 structure has been also observed in LEED studies of 0.5 ML (monolayer) NiO that disappears at 1.5 ML thickness.<sup>9</sup> The formation of a 2×1 layer and the preferential growth of double-layer islands during the initial growth stages of NiO on Ag(001) has been also reported in a SPA-LEED study.<sup>12</sup> As far as the preparation procedure is concerned, it has been shown that the use of more aggressive oxidizing agents like NO<sub>2</sub> leads to high-quality thin films, with a 1×1 structure since the first NiO ML.<sup>6,15</sup> On a larger thickness scale, both the structure and composition of NiO films deposited by dc reactive sputtering Ni in an Ar<sup>+</sup>-O<sub>2</sub> mixed atmosphere on Si substrate were found to depend on the oxygen content in the gas mixture.<sup>16</sup>

The aim of the present work was to investigate the film composition and structure, with emphasis on the occurrence of different reconstructions in the very initial stage of the NiO growth on Ag(001) substrate, in dependence on the procedure of reactive growth and in particular on the relative amount of oxygen and nickel flux on the substrate surface. The oxide structural arrangement has been monitored both in reciprocal and in direct space by LEED and PDME,<sup>17-19</sup> while chemistry and composition have been studied by core-level x-ray photoemission spectroscopy (XPS).

## EXPERIMENT

The Ag(001) substrate was prepared by repeated cycles of sputtering (Ar<sup>+</sup> ions, 600 eV, 0.8 μA/cm<sup>2</sup>) and annealing at 400 °C. Oxide films were prepared in an UHV chamber (base pressure 5×10<sup>-11</sup> Torr) using a Knudsen cell for Ni evaporation and a gas inlet for simultaneous O<sub>2</sub> exposure. Ni atoms were deposited at a rate of 0.1–0.6 Å/min. The rate was

measured by a quartz microbalance. The flux of  $O_2$  was localized on the substrate by a nozzle located close (10 mm) to the surface. The  $O_2$ -to-Ni flux ratio will be referred to as  $n$  and was varied in the 30–800 range. The  $n$  parameter has been evaluated after several assumptions. The number of  $O_2$  molecules introduced in the growth system per unit time has been estimated by the product of the  $O_2$  partial pressure ( $4 \times 10^{-8}$  Torr) and the pumping speed of the system (500 l/s). Since a nozzle was used to direct the gas flow to the sample surface, we assume that all the introduced molecules impinge on the surface. The Ni atom flux has been measured by the quartz microbalance placed at the sample position. These evaluations are quite rough with respect to the absolute value of  $n$ : however, they are significant as far their relative values are concerned. The NiO deposition rate was about 0.1–0.5 ML/min, as evaluated by the Ni deposition rate and the Ni atomic density in the oxide. During deposition, the substrate temperature was held to 190 °C. While in Refs. 7–10 and 12 a RT growth is performed, in Refs. 15 and 6 a higher substrate temperature is suggested for obtaining higher-quality films. With an increased substrate temperature, a higher dose of  $O_2$  or a more reactive agent<sup>15,6</sup> is needed for oxidizing the Ni. At the same time, the substrate temperature could play a role in the Ni-Ag alloying rate. The product of NiO rate and deposition time will be referred to as the nominal thickness. Quantitative XPS analysis was used to check the reliability and the accuracy of the Ni deposition rate measured by the quartz microbalance: the results of both methods agree within 10%. The Ni-Ag alloying effect concerns a small fraction of the total area (if we exclude the  $n=30$  sample) and therefore cannot effect the actual height of the thick films.

PDME measurements<sup>17–19</sup> consist in measuring the electron-excited Auger signal intensity as a function of the beam incidence angle. The incident beam intensity is modulated by the ordered crystal structure by a focusing and diffraction process similar to that occurring to the outgoing photoelectrons in x-ray photoemission spectroscopy (XPD). The incident beam intensity modulation is reproduced by the measured Auger signal. The PDME experiments were performed by a PHI 590A spectrometer with the cylindrical mirror analyzer (CMA) operated in the first derivative mode (0.6% resolution, 15-V modulation) and the coaxial electron gun operated at 5 keV and 1  $\mu$ A. A computer-controlled manipulator provided the rotation of the sample in front of the analyzer with an accuracy of 0.1°. Auger intensities from the film and substrate were collected as a function of the incidence angle of the primary beam which was changed by steps of 1° along the [100] substrate azimuth. The angular acceptance of the CMA was proved to be large enough to smear out the outgoing electron diffraction features.<sup>17</sup> LEED measurements were performed using a WA Technology rear-view, four-grid apparatus, with the electron gun operated at 168 eV to minimize the contribution from the Ag substrate;<sup>20</sup> images were recorded using a computer-controlled 16-bit charge-coupled-device (CCD) camera. The position of the sample in front of the LEED was reproduced with an accuracy of  $\pm 0.01$  mm. XPS measurements were performed using a nonmonochromatic Al  $K\alpha$  source and an hemispheri-

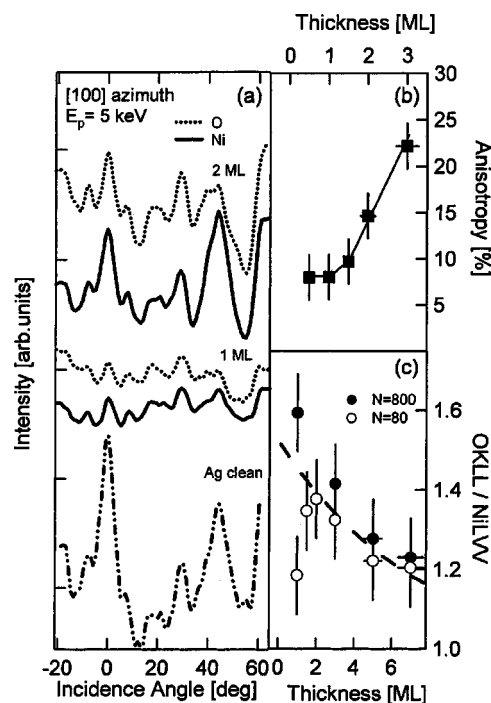


FIG. 1. (a) IAD's of Ni LVV and O KLL Auger signals along the [100] azimuth on the (001) surface of 1-ML and 2-ML NiO films prepared by the  $n=80$  procedure; the Ag MNN IAD is also shown, measured on the clean substrate. (b) Intensity anisotropy of the [001] peak as a function of NiO thickness, in the Ni LVV IAD. (c) O KLL/Ni LVV Auger intensity ratio vs thickness of NiO films prepared by the  $n=80$  and 800 procedures (open and solid dots, respectively).

cal analyzer Omicron EA125. Photoemission spectra were taken with a resolution of 2 eV, measured at the Ag Fermi edge.

## RESULTS AND DISCUSSION

The NiO growth mode has been first monitored by PDME. The intensity of the relevant Auger peaks of the overlayer has been measured as a function of the incidence angle of the primary beam along the [100] substrate azimuth for NiO films of increasing thickness. The intensity angular distributions (IAD's) of O KLL and Ni LVV peaks are shown in Fig. 1(a) for 1- and 2-ML films prepared with  $n=80$ . Similar results have been obtained on NiO films prepared with  $n=800$ . The Ag MNN IAD measured on the clean substrate is also shown (bottom curve). In the 2-ML IAD's, maxima in the Auger emission intensity occur, due to the forward focusing of the primary intensity along low-index chains of the rocksalt NiO structure. The peaks at 0° and about 45° correspond to the beam alignment along the dense [001] and [101] chains, respectively. The most direct way to follow the tetragonal distortion in cubic materials is by measuring the position of the [101] forward-focusing peak in the (100) azimuth.<sup>21</sup> The forward-focusing peak related to the close-packed [101] chain actually occurs at a lower angle (43.9°) with respect to the ideal rocksalt value of 45°. The angular separation between the [101] forward peak and the [001] one is related to the ratio between the in-plane (a) and out-of-plane (c) parameters of the NiO rocksalt structure.

The angular position of the [101] peak indicates the occurrence of a tetragonal distortion of the cubic cell ( $a/c = 0.96$ ) to accommodate the lattice mismatch between the Ag and NiO equilibrium structure. Assuming a Poisson ratio value for NiO of 0.31,<sup>22</sup> the calculated  $a/c$  value for the in-plane compressed NiO film is 0.9594, in good agreement with our experimental findings.

The strength of the individual features in the IAD's is quantitatively described by the intensity anisotropy, defined as  $2(I_{\max} - I_{\min}) / (I_{\max} + I_{\min})$ , where  $I_{\max}$  ( $I_{\min}$ ) is the maximum (minimum) signal intensity measured crossing the considered feature. The anisotropy of the [001] forward-focusing peak in the Ni LVV IAD is reported versus thickness of the NiO film in Fig. 1(b). Data refer to the  $n = 80$  film, but they are representative also of the  $n = 400$  and 800 films. The nonzero (8%–10%) Ni and O intensity anisotropy observed in the submonolayer and ML range is ascribed to the nonisotropic contribution of the backscattered electrons to the ionization of the outermost layers, as first discussed for Si submonolayers on Mo(100) and (110) (Ref. 23) and recently reported for ultrathin Ag layers on Cu(001) (Ref. 24) and Co layers on Fe(001) (Ref. 25). Backscattered electrons are in fact modulated in intensity by the substrate structure, according to the scattering-interference process experienced by the primary beam, and significantly contribute to the ionization of the outermost layer. In the presence of a significant fraction of double layer, forward focusing occurs along specific directions and a sudden increase of the anisotropy, up to nearly the double of the backscattering value, is expected.<sup>25</sup> The low, constant value of the overlayer signal anisotropy for 0.5 and 1 ML deposition and the rise of the anisotropy for deposition larger than 1.5–2 ML both indicate that, if any, the occurrence of double or multiple layers in the nominally 1-ML-thick films is a minor effect and that a two-dimensional growth substantially occurs.

The O *KLL*/Ni *LVV* intensity ratio was obtained by averaging the PDMEE intensity angular distributions in order to reduce the effects of electron diffraction on the quantitative analysis of the Auger spectra and is shown in Fig. 1(c) as a function of the NiO nominal thickness for both the  $n = 80$  and 800 procedures. The expected O *KLL*/Ni *LVV* value has been calculated (dashed curve) with the assumption of a layer-by-layer growth of a stoichiometric oxide, also taking into account the different inelastic mean free paths of the O *KLL* (11 Å) and Ni *LVV* (17 Å) electrons<sup>26</sup> (this difference is actually responsible for the increasing value of the intensity ratio as the film thickness reduces). At 1 ML deposition a marked effect of the deposition procedure on the film composition is observed, while for deposition larger than 2 ML the film composition is nearly independent of the  $n$  value.

In Fig. 2, the LEED patterns ( $E_p = 168$  eV, normal incidence) of the Ag(001) substrate and of 1-ML Ni/Ag(001) [panels (a) and (b), respectively] are compared to the pattern of 1 ML NiO/Ag(001) film prepared with different oxygen-to-nickel flux ratios [ $n = 30, 80,$  and 800, panels (c)–(e)], as well as to the pattern of 2-ML NiO/Ag(001) film prepared with  $n = 80$  [panel (f)]. The corresponding spot profiles of the LEED intensity along the [110] substrate direction are also shown panels (a')–(f'). In order to minimize the contribu-

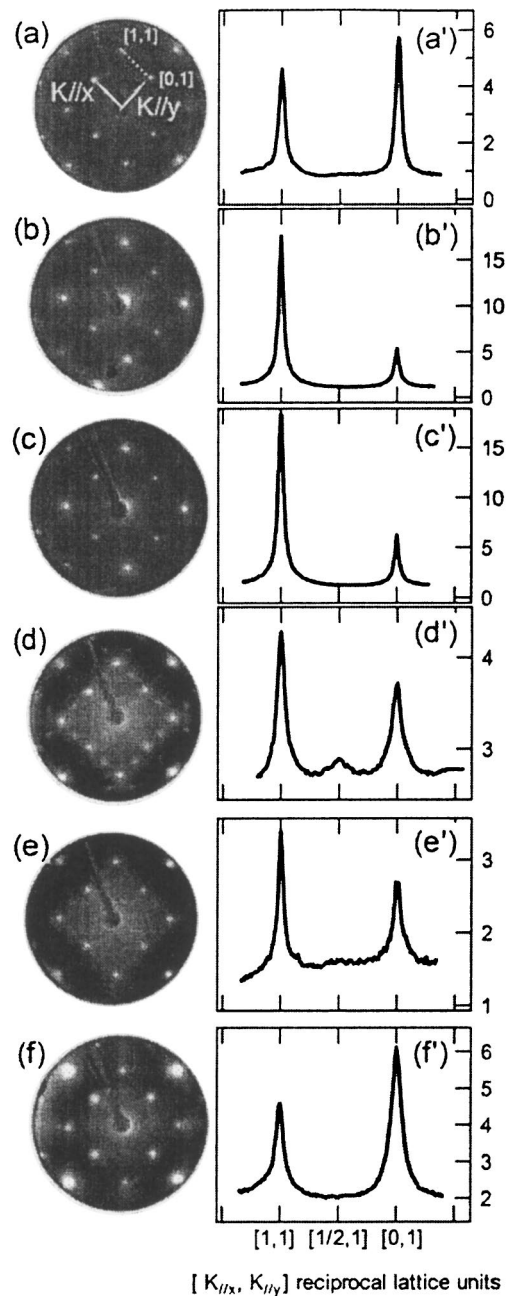


FIG. 2. Left: LEED patterns (168 eV). Ag(001) substrate [panel (a), where the white arrows indicate the unit cell in reciprocal space], 1-ML Ni/Ag(001) [panel (b)], 1-ML NiO/Ag(001) film prepared with different oxygen-to-nickel flux ratio (30, 80, and 800 [panel (c)–(e)] and 2-ML NiO/Ag(001) film prepared with  $n = 80$  [panel (f)]. Right: the corresponding polar distributions of the LEED intensity along the white path indicated in panel (a).

tion from the Ag substrate,<sup>20</sup> a beam energy value close to the extinction of the (10) and (11) spots was chosen. This leads to the unusually large background to signal ratio in panel (a'). The film prepared with the  $n = 800$  procedure exhibits a substratelike ( $1 \times 1$ ) pattern with spot width slightly larger if compared to the spots of the Ag(001) surface, indicating the growth of large, well-ordered NiO(001) domains with the NiO[100]//Ag[100] epitaxial relationship

and an almost full coverage of the Ag substrate. However, the spot-to-background ratio is significantly decreased with respect to the clean substrate, suggesting the nucleation of point defects. LEED patterns allow the measure of the in-plane lattice parameter of the outermost layer. The accuracy of the measurement is enhanced by a careful positioning of the surface in the focal point of the screen and by averaging over distances between different spots in the LEED pattern. From patterns (a) and (e) of Fig. 2 it has been found that a nearly ideal in-plane matching occurs between the overlayer and substrate.

At variance with the  $n=800$  procedure, the  $n=80$  procedure results in a fourfold-symmetric LEED pattern with half-order extra spots along the  $[110]$  directions, beside the  $(00)$ ,  $(10)$ , and  $(20)$  integer spots. This indicates a  $(2 \times 1)$  overlayer reconstruction in two orthogonal domains. Both the width of the integer spots and the background intensity are slightly larger compared to the  $n=800$   $(1 \times 1)$  pattern, suggesting a lower degree of long-range order in the  $n=80$  film. At 2 ML NiO deposition the  $(2 \times 1)$  reconstruction disappears [panels (f) and (f')] and the  $(10)$ -to- $(11)$  spot intensity ratio becomes larger than 1, thus evolving toward the value measured on thicker (20 ML) films.

The occurrence of a  $(2 \times 1)$  reconstruction has been already observed by LEED (Ref. 9) and STM (Ref. 10) for submonolayer NiO films prepared at RT on Ag(001) substrate by Ni deposition in a background oxygen atmosphere of about  $1 \times 10^{-6}$  mbar. It has been also reported that the  $2 \times 1$  phase disappears upon annealing of the RT-deposited film.<sup>10</sup> However, an explicit correlation between the occurrence of this structure and the preparation procedure has never been established up to now. Comparison between the  $n=80$  and 800 results indicates that the  $(2 \times 1)$  structure originates in an oxygen deficiency during the growth. However, we notice that this structure cannot be detected in the oxide layer prepared with the  $n=30$  procedure. More generally, in terms of both the peak width and the  $(10)$ -to- $(11)$  spot intensity ratio the  $n=30$  film pattern closely resembles the 1-ML Ni film pattern. The  $(2 \times 1)$  LEED pattern observed in ultrathin NiO layers has been sometimes ascribed to a superstructure of adsorbed oxygen on NiO.<sup>9</sup> This hypothesis seems not favored by the extremely low sticking coefficient of O on Ag at temperatures above RT.<sup>27</sup> This is confirmed by STM data<sup>10</sup> and an alternative model has been proposed for a  $(2 \times 1)$  O/Ni/Ag(001) precursor structure, where protruding Ni rows alternate with rows which are located somewhat deeper and the oxygen atoms are located in threefold hollow sites.<sup>10</sup> This model is, however, not fully compatible with the results of a recent *ab initio* density functional study of the interfacial geometry (adsorption sites and distances) of the 1-ML NiO/Ag(001) system.<sup>28</sup> LEED intensities of the  $(2 \times 1)$  NiO structure of 1-ML NiO films reactively prepared on Ag(001) with low oxygen dosage have been measured,<sup>29</sup> but a quantitative structural analysis is still in progress.

The 1-ML oxide films prepared at different oxygen-to-nickel flux ratios were found to exhibit marked differences in the Ni 2*p* photoemission spectra. Ni 2*p* spectra, whose background has been subtracted by the Shirley algorithm, are shown in Fig. 3 for a wide range of  $n$  values from 30 to 800.

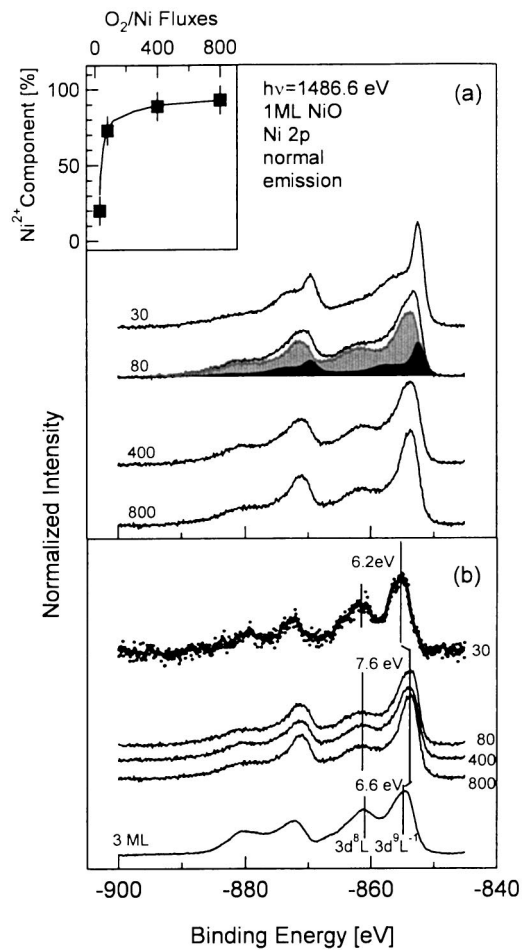


FIG. 3. (a) Background subtracted Ni 2*p* photoemission spectra of 1-ML oxide film prepared at increasing O<sub>2</sub>-to-Ni flux ratio from 30 to 800. Spectra have been collected in normal take-off geometry and were normalized to their area. Ni<sup>0</sup> and Ni<sup>2+</sup> spectral contributions to the overall Ni 2*p* line shape at  $n=80$  are shown (black and gray areas, respectively). (b) Ni<sup>2+</sup> spectral contributions to the Ni 2*p* line shape at increasing O<sub>2</sub>-to-Ni flux ratio. The Ni 2*p* photoemission spectrum of 3-ML NiO film prepared with the  $n=80$  procedure is also shown (bottom curve). Inset shows the percent weight of the Ni<sup>2+</sup> contribution to the overall Ni 2*p* emission as a function of the  $n$  value.

On moving the  $n$  value from 800 to 80 we mainly notice that the  $3d^9L^{-1}$ -related  $2p_{1/2}$  and  $2p_{3/2}$  peaks progressively increase in width and shifts to lower binding energy (BE) and that the  $3d^8L$ -related satellites become less separated from the main peak. As the  $n$  value further reduces to 30, the Ni 2*p* line shape clearly evolves toward the metallic Ni line shape. This trend suggests that the 1-ML NiO spectrum is a weighted superposition of contributions from both metallic and oxidized Ni atoms. Changes of the overall Ni 2*p* line shape is therefore ascribable to changes in the relative intensity of these two contributions and/or to changes in the spectrum of the oxidized Ni phase.

To get a reference spectra for the metallic component, the Ni 2*p* line shape of 1-ML Ni/Ag(001) film has been measured in the same conditions in a separate experiment. The detailed study of the Ni/Ag(001) interface is beyond the

scope of this paper. We subtracted the metallic component from the Ni 2*p* line shape of the 1-ML NiO/Ag(001) films, and the remaining spectral contributions have been ascribed to the oxide phase. The criterion was to subtract the largest amount of metallic component, provided that the spectral intensity in the 845–890 eV range remains non-negative. An example of the separation procedure is shown in Fig. 3(a). The Ni oxide spectral contributions to the overall 1-ML Ni 2*p* spectra are comparatively shown in Fig. 3(b). We notice that the shape of the oxide-related 2*p* emission is very similar for all the 1-ML films (with the exception of the  $n=30$  film, which will be discussed later), indicating that a unique oxidized phase is formed, irrespective of the  $n$  value, and that changes in the Ni 2*p* line shape associated with changes in the oxygen-to-nickel flux ratio are mainly due to changes in the relative amount of metallic Ni atoms in the so-called 1-ML NiO film. The weight of the Ni<sup>2+</sup> contribution to the overall Ni 2*p* emission is shown in the inset of Fig. 3 as a function of the  $n$  value. For  $n=400$  or larger, this contribution is of the order of 90%, but it significantly reduces for  $n=80$  and becomes largely minor (about 20%) for  $n=30$ . We conclude that the effect of the oxygen dosage on the composition of the 1-ML-deposited film is dramatic for an oxygen-to-nickel flux ratio lower than about 100, but it is less important for a ratio larger than about 300.

The presence of a relevant fraction of metallic Ni atoms for low values of  $n$  is possibly due to the competing effect of the Ni dissolution kinetic in the Ag substrate with respect to the Ni oxidation kinetic. Both experiments and simulations showed in fact for the Ni/Ag(001) interface a “surfactant-like” behavior that consists of the formation of layers or clusters of Ni buried below some Ag floating monolayers.<sup>30–32</sup> A similar effect has been observed for different metals like Rh (Ref. 33), Cr (Ref. 34), and Fe (Ref. 35) on Ag(001). Therefore in presence of an O<sub>2</sub> molecules deficiency with respect to Ni atoms, a fraction of the deposited Ni atoms dissolve into the Ag substrate, thus maintaining a metallic character. In a separate experiment (not reported here) the actual occurrence of such an intermixing has been observed by a comparative sputter profile of both the Ni/Ag(001) and NiO/Ag(001) interfaces. The Ni dissolution effect is limited to the initial stage of the deposition. Actually, the spectral weight of the metallic Ni component for the  $n=80$  deposition passes from 28% for 1 ML to 10% for 3 ML. This decrease is consistent with the assumption that the deposition of the subsequent layers do not contribute to the metallic Ni signal. Rather, they attenuate the metallic fraction that dissolved into the substrate in the early stage of the deposition.

It should be mentioned that the (2×1) phase cannot be ascribed to an arrangement of the large fraction of metallic Ni atoms in the  $n=80$  film. In fact, there is no evidence of the occurrence of this phase in the LEED pattern of the  $n=30$  film, where the fraction of metallic Ni is even larger. Therefore the (2×1) phase is ascribable to the oxidized portion of the film, but it is only observed in presence of metallic Ni.

Oxide spectral contributions look very similar in shape for all the films prepared with an  $n$  value of 80 or larger. Rel-

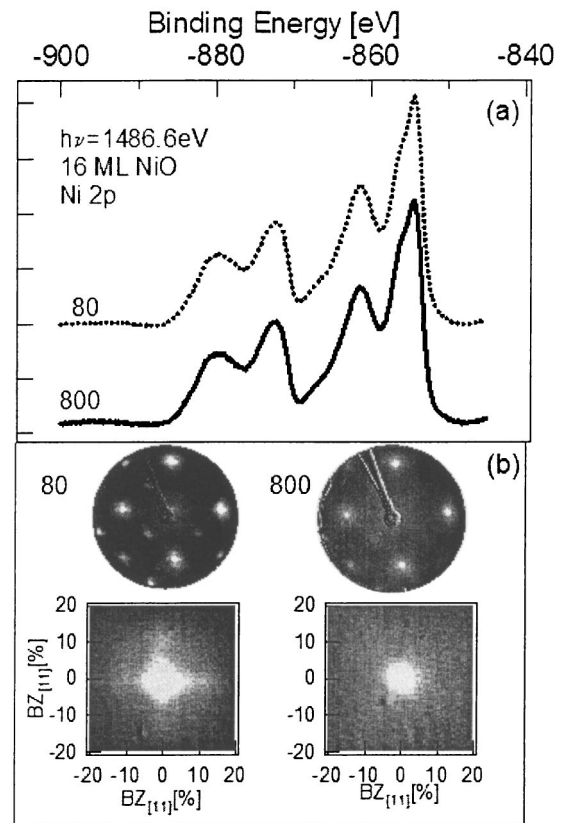


FIG. 4. Ni 2*p* photoemission spectra (a) and 148-eV LEED patterns (b) of 16-ML NiO films prepared by  $n=80$  and 800 procedures. The shape of the (1,1) spot is shown in detail in the bottom panels.

evant spectral parameters—namely, the BE of the  $3d^9L^{-1}$  peaks and the energy separation between the  $3d^9L^{-1}$  and  $3d^8L$  features—are in agreement with the data reported in the literature for 1-ML NiO films.<sup>6,36</sup> The reduced intensity of the  $3d^8$  satellites with respect of the  $3d^9L^{-1}$  main peaks and the absence of the nonlocal screening satellite in the  $3d^9L^{-1}$  peaks are additional fingerprints of a Ni 2*p* emission ascribable to an ultrathin NiO layer. The relative intensity of the  $3d^8L$  satellites in fact starts to increase in the 3-ML spectrum [Fig. 3(b), bottom curve], and the nonlocal screening satellite becomes evident only at 5 ML thickness (not shown here).

The oxide spectral contribution to the Ni 2*p* emission from the film prepared with the  $n=30$  procedure exhibits a quite different shape [top curve in Fig. 3(b)]. Having in mind that in this case only 20% of the deposited Ni atoms react with oxygen to form a Ni oxide, we are possibly dealing with 1-ML-thick NiO aggregates of very small lateral dimensions. The line-shape difference with respect to the  $n=80$ –800 is therefore ascribable to the further (lateral) confinement in addition to the vertical confinement of the ML films. As far as the BE, the splitting, and the relative intensities of the main lines and satellites are concerned, the  $n=30$  spectrum closely resembles that of diluted NiO, as measured on Ni<sub>x</sub>Mg<sub>1-x</sub>O mixed crystals or powders.<sup>4,37</sup> The LEED pattern [panels (c) and (c') of Fig. 2], strictly similar to the

1-ML Ni pattern [panels (b) and (b') of Fig. 2], suggests that both the amount of oxidized Ni (0.2 ML from XPS analysis) and the reduced lateral dimensions of the NiO aggregates are too small to give a detectable contribution to the LEED pattern.

The effects of a different oxygen dosage during Ni deposition on the composition and structure of the NiO films seem to be confined to the very initial phase of the growth. However, some effects were found to persist at a very large coverage. In Fig. 4, the XPS spectra and LEED patterns of 16-ML NiO/Ag(001) films prepared with the  $n=80$  and 800 procedures are compared. The Ni  $2p$  line shape is very similar for the two cases and fully consistent with the spectra reported in the literature for NiO thick films or bulk samples. LEED patterns, however, in spite of the similar,  $(1 \times 1)$  four-fold symmetry with respect to the surface normal, exhibit relevant differences as far as the spot shape is concerned. Both the (11) and (10) spots in the  $n=80$  pattern are surrounded by four additional spots in the  $\langle 100 \rangle$  substrate directions. The separation of the satellites from the main spots is about 20% of the Brillouin zone (BZ). Similar features have been already observed in NiO films and also in MgO films whose thickness is larger than a critical value (several ML's) and have been interpreted as induced by a mosaic structure that forms in the oxide film to relax the misfit strain by introducing interfacial dislocations.<sup>12,38</sup> Following this interpretation, the results of Fig. 4(b) suggest a larger critical thickness for NiO films reactively grown with a larger oxygen dosage or that there is smoother way to release the strain, different from mosaics formation. This is possibly ascribable to the already mentioned, different extent of the interfacial disruption by Ni-Ag exchange in dependence of the different growth conditions, either via a different elastic coupling be-

tween the substrate and film or via a different ability to nucleate dislocations in presence of a different interfacial roughness.<sup>39</sup>

## CONCLUSIONS

In summary, we have shown that the oxygen-to-metal flux ratio strongly influences the structure and composition of 1-ML Ni oxide films prepared by Ni deposition on the Ag(001) surface in a background O<sub>2</sub> atmosphere. For low oxygen dosage, a relevant fraction (up to 80%) of the deposited Ni atoms shows a metallic character, while only a minor fraction reacts with oxygen to form Ni oxide. The layers show a  $2 \times 1$  reconstruction that disappears as the thickness of the film increases. For a large oxygen dosage, the fraction of metallic Ni in the deposited film strongly reduces (down to about 8%) and the layer exhibit a  $(1 \times 1)$  structure. The oxide-related Ni  $2p$  line shape indicates that all the NiO films are actually 1 ML thick and that for very low oxygen dosage a severe lateral confinement of the NiO aggregates also occurs.

Finally, differences in the 1-ML films induced by the different oxygen dosages during the growth also affect the structure of thicker NiO layers, in terms of strain relaxation.

## ACKNOWLEDGMENTS

The authors are indebted to S. Altieri, A. Atrei, and G. Rovida for useful discussions. Financial support by Istituto Nazionale per la Fisica della Materia (Advanced Research Project ISADORA) and by Ministero dell'Istruzione, dell'Università e della Ricerca (Progetti FIRB) is gratefully acknowledged.

\*Corresponding author. FAX: +39 059 205 5235. Electronic address: giovanardi.chiara@unimore.it

<sup>1</sup>H. J. Freund, H. Kühlenbeck, and V. Staemmler, Rep. Prog. Phys. **59**, 283 (1996).

<sup>2</sup>M. Bäumlner and H. J. Freund, Prog. Surf. Sci. **61**, 127 (1999).

<sup>3</sup>H. D. Chopra, B. J. Hockey, P. J. Chen, W. F. Egelhoff, Jr., M. Wuttig, and S. Z. Hua, Phys. Rev. B **55**, 8390 (1997).

<sup>4</sup>S. Hufner, Adv. Phys. **43**, 183 (1994).

<sup>5</sup>B. Fromme, *d-d Excitations in Transition-Metal Oxides*, Springer Tracts in Modern Physics, Vol. 180 (Springer, Berlin, 2001).

<sup>6</sup>S. Altieri, Ph.D. thesis, Groningen University, 1999.

<sup>7</sup>K. Marre and H. Neddermeyer, Surf. Sci. **287-288**, 995 (1993).

<sup>8</sup>K. Marre, H. Neddermeyer, A. Chassè, and P. Rennert, Surf. Sci. **357-358**, 233 (1996).

<sup>9</sup>F. Muller, R. de Masi, P. Ser, D. Reinicke, M. Stadtfelt, and H. Hufner, Surf. Sci. **459**, 161 (2000).

<sup>10</sup>T. Bertrams and H. Neddermeyer, J. Vac. Sci. Technol. B **14**, 1141 (1996).

<sup>11</sup>I. Sebastian, T. Bertrams, K. Meinel, and H. Neddermeyer, Faraday Discuss. **114**, 129 (1999).

<sup>12</sup>J. Wollschläger, D. Erdös, H. Goldbach, R. Hopken, and K. M. Schröder, Thin Solid Films **400**, 1 (2001).

<sup>13</sup>C. Giovanardi, A. di Bona, S. Altieri, P. Luches, M. Liberati, F. Rossi, and S. Valeri, Thin Solid Films **428/1-2**, 195 (2003).

<sup>14</sup>P. Luches, S. Altieri, C. Giovanardi, T. S. Moia, S. Valeri, F. Bruno, L. Floreano, A. Morgante, A. Santaniello, A. Verdini, R. Gotter, and T. Hibma, Thin Solid Films **400**, 139 (2001).

<sup>15</sup>S. D. Peacor and T. Hibma, Surf. Sci. **301**, 11 (1994).

<sup>16</sup>I. Hotovy, D. Buc, S. Hascik, and O. Nennowitz, Vacuum **50**, 41 (1998).

<sup>17</sup>S. Valeri, A. di Bona, and G. C. Gazzadi, Surf. Interface Anal. **21**, 852 (1994).

<sup>18</sup>A. Stuck, M. Nowicki, S. Mroz, D. Naumovic, and J. Osterwalder, Surf. Sci. **306**, 21 (1994).

<sup>19</sup>S. Valeri and A. di Bona, Surf. Rev. Lett. **4**, 141 (1997).

<sup>20</sup>The  $I(V)$  data repository, www.matscieng.sunysb.edu/ivdata

<sup>21</sup>S. A. Chambers, Adv. Phys. **40**, 357 (1991).

<sup>22</sup>*Elastic, Piezoelectric, Pyroelectric, Piezooptic, Electrooptic Constants, and Nonlinear Dielectric Susceptibilities of Crystals*, edited by K.-H. Kellwege and A.M. Hellwege, Landolt-Börnstein, New Series, Group III, Vol. 11, (Springer-Verlag, Berlin, 1979), p. 28.

<sup>23</sup>M. V. Gomoyunova, S. L. Dudarev, and I. I. Pronin, Surf. Sci. **235**, 156 (1990).

<sup>24</sup>M. Nowicki and P. Krupa, Vacuum **48**, 313 (1997).

<sup>25</sup>A. di Bona, P. Luches, A. Borghi, F. Rossi, and S. Valeri, Surf. Rev. Lett. **6**, 599 (1999).

<sup>26</sup>S. Tanuma, C. J. Powell, and D. R. Penn, Surf. Interface Anal. **21**, 165 (1994).

- <sup>27</sup>M. Rocca, L. Savio, L. Vattuone, U. Burghaus, V. Palomba, N. Novelli, F. Buatier de Mongeot, U. Valbusa, R. Gunnella, G. Comelli, A. Baraldi, S. Lizzit, and G. Paolucci, *Phys. Rev. B* **61**, 213 (2000) and references therein.
- <sup>28</sup>S. Casassa, A. M. Ferrari, M. Busso, and C. Pisani, *J. Phys. Chem. B* **106**, 12 978 (2002).
- <sup>29</sup>M. Caffio, B. Cortigiani, G. Roviada, A. Atrei, C. Giovanardi, and A. di Bona, *Surf. Sci.* **531**, 368 (2003).
- <sup>30</sup>J.-M. Roussel, A. Saul, and G. Treglia, *Phys. Rev. B* **55**, 10 931 (1997).
- <sup>31</sup>K. S. Lee, S. H. Kim, H. G. Min, J. Seo, and J.-S. Kim, *Surf. Sci.* **377-379**, 918 (1997).
- <sup>32</sup>B. Aufray, H. Giordano, B. Legrand, and G. Treglia, *Surf. Sci.* **307-309**, 531 (1994).
- <sup>33</sup>S.-L. Chang, J.-M. Wen, P. A. Thiel, S. Gunther, J. A. Meyer, and R. J. Behm, *Phys. Rev. B* **53**, 13 747 (1996).
- <sup>34</sup>M. C. Hanf, C. Krembel, and G. Gewinner, *Surf. Sci.* **519**, 1 (2002).
- <sup>35</sup>M. Canepa, E. Magnano, A. Campora, P. Cantini, M. Salvietti, and L. Mattera, *Surf. Sci.* **352**, 36 (1996).
- <sup>36</sup>D. Alders, F. C. Voogt, T. Hibma, and G. A. Sawatzky, *Phys. Rev. B* **54**, 7716 (1996).
- <sup>37</sup>S. Altieri, L. H. Tjeng, A. Tanaka, and G. A. Sawatzky, *Phys. Rev. B* **61**, 13 403 (2000).
- <sup>38</sup>M. Schulze and R. Reissner, *Surf. Sci.* **482-485**, 285 (2001).
- <sup>39</sup>L. Dong, J. Schnitker, R. W. Smith, and D. J. Srolovitz, *J. Appl. Phys.* **83**, 217 (1998).